Tuning Photophysical Properties of Acceptor-Donor-Acceptor Di-2-(2-oxindolin-3-ylidene) Malononitrile Materials via Extended π-Conjugation: A Joint Experimental and Theoretical Study

Shiwei Ren, Amirhossein Habibi, Pingping Ni, Yuexing Zhang, Abderrahim Yassar

Tuning Photophysical Properties of Acceptor–Donor–Acceptor Di-2-(2-oxindolin-3-ylidene) Malononitrile Materials via Extended π–Conjugation: A Joint Experimental and Theoretical Study

Shiwei Ren,[a] Amirhossein Habibi,[b] Pingping Ni,[b] Yuexing Zhang*[c] and Abderrahim Yassar*[b]

[a] *Zhuhai Fudan Innovation Institute, Guangdong-Macao in-depth cooperation zone in Hengqin 518057, PR China; Laboratory of Molecular Materials and Devices, Department of Materials Science, Fudan University, Shanghai 200433, PR China.*

[b] *LPICM, CNRS, Ecole Polytechnique, Institut Polytechnique de Paris, Route de Saclay, 91128 Palaiseau, France. E-mail: abderrahim.yassar@polytechnique.edu.*

[c] *Shandong Provincial Key Laboratory of Monocrystalline Silicon Semiconductor Materials and Technology, Shandong Universities Engineering Research Center of Integrated Circuits Functional Materials and Expanded Applications, College of Chemistry and Chemical Engineering, Dezhou University, Dezhou 253023, Shandong, PR China. E-mail: zhangyuexing@sdu.edu.cn.*

ABSTRACT

Organic semiconductor (OSC) materials with a high electron affinity are required for many optoelectronic applications. In this work a series of twelve novel acceptor-donor-acceptor (A–D–A) materials with low-lying LUMO energy levels are designed, synthesized, and characterized. In this strategy, two acceptor dyes, isatin and its dicyanovinyl derivatives are connected by various π–bridges. We have varied the π–conjugation length of the central core and altered the linkage position of the acceptor core (4-position vs. 6-position of the phenyl ring of the isatin moiety) to study the effect of extended π–conjugation and point of linkage of the acceptor on optical and electrochemical properties of the new dyes. Density functional theory (DFT) and time-dependent DFT (TD–DFT) studies have been performed to gain an insight into their electronic properties by determining the energy levels and maps of the HOMO, LUMO as well as HOMO–LUMO gap (energy differences between the highest occupied and lowest unoccupied molecular orbitals). Our findings demonstrate that with increasing the acceptor strength and π–conjugation length of the

core, the wavelength of the longest absorption maximum as well as their respective extinction coefficients are enhanced, which resulted in band-gap reduction either by lowering the LUMO and or raising the HOMO energy level of the molecules. Space-charge-limited current measurements (SCLC) were investigated to probe the electron mobility of these molecules. Electron only devices were fabricated by the spin-coating and the trap-limited electron mobility was calculated using Mott-Gurney law. **10a** exhibited an intrinsic moderate electron mobility of 8.94×10^{-4} cm^2 V^{-1} s^{-1}. The potential practical utility of these materials as an electron-transport material for perovskite solar cells (PSCs) has been demonstrated.

Keywords: acceptor-donor-acceptor (A–D–A) materials, π–conjugation, electron mobility, perovskite solar cells.

1. Introduction

OSC materials with low-lying LUMO energy levels are particularly interesting for many optoelectronic applications, in particular for n-channel organic field-effect transistors (OFET), as non-fullerene acceptors and electron transporting materials for perovskite solar cells [1]. To date, tremendous efforts have been devoted to explore new building blocks for the fabrication of novel n-type OSC. One key requirement for developing n-type OSC is the high electron affinity, which facilitates electron injection and stabilizes injected electrons. This is usually expressed in terms of the energy level of the LUMO, which should be sufficiently low-lying (≤ –3.5 eV) to facilitate electron injection from the cathode. The chemical structure and the nature of the electron-withdrawing building block are used mainly to settle the LUMO energy level.

Various building blocks have been employed to construct new n-type OSC. Among them, bis-lactam are of particular interest owing to their strong electron-withdrawing ability and dipolar carbonyl groups which facilitate strong intermolecular interactions [2, 3]. Based on the bis-lactam design strategies, various novel electron-deficient building blocks for high-performance OSC have been reported [4, 5]Isatin and its dicyanovinyl derivatives belong to this family, and they are good synthetic precursors of many natural products and also promising n-type acceptor-donor-acceptor (A–D–A)–type OSC due to their planar framework with two electron-withdrawing carbonyl groups [6-8]. In the past, various D-A type dyad and triad architectures have been designed and synthesized, their photophysical properties are largely influenced by the way in which the dyad and triad systems is constructed (AD, DAD, ADA, etc.). Through appropriate chemical modification of isatin core, a significant number of n-type OSC with a low LUMO energy level have been reported. Kuo and co-workers reported molecular design strategies of three di-2-(2-oxindolin-3-ylidene) malononitrile derivatives (**I–1a**, **1b**, and **1c** in Figure 1) with various numbers of nitrogen substituents on the phenyl rings for use as n-type OFET-materials [9]. They demonstrated by selectively controlling the number of nitrogen atoms introduced on the phenyl group, that the LUMO energy level could be fine-tuned from –4.02 eV for the unsubstituted to –4.16 eV for the disubstituted derivative. The introduction of the amine functionality not only lowers the LUMO level but also enhances the molecule's coplanarity, which results in a moderate electron mobility of 0.059 cm^2 V^{-1} s^{-1}. However, the replacement of a phenyl ring with a pyridine had a slight effect on the

absorption spectra. The same group later reported the synthesis and characterization of two derivatives of fused angular-shaped naphthalene bis-isatin (**I–2**) core [10]. These new derivatives showed a low-lying LUMO energy level of –4.25 eV, lower than that of previously reported, making them suitable materials for air-stable n-type OSC. These naphthalene derivatives, **I–2** displayed a broad absorption with two main absorption bands at 300−450 and 550−800 nm, assigned as the π–π* and intramolecular charge transfer (ICT) transitions, respectively. Benzodipyrrole-2,6-dione-3,7-diylidenedimalononitrile, **I–3**, which was a structural analogue to **I–2** by replacing naphthalene core with a phenyl moiety, was recently reported and its electrochemical behavior was investigated by cyclic voltammetry (CV) [11]. The CV results showed reversible reduction−oxidation processes and the LUMO levels were estimated at –4.42 eV. To analyse the effect of acceptor strength on the optoelectronic properties, Mori et al. synthesized **I–4a** in which the phenyl ring of the isatin core is replaced by a thiophene ring [12]. **I–4b** exhibited a considerably stronger electron deficiency properties than that found in **I–4a** parent, with a deep LUMO level of –4.28 eV. Compared with **I–4a**, the absorption spectra of thienoisatin derivatives displayed a broader and red-shifted features with a λ_{max} of 650 nm. The red-shift was due to an increased D-A character of **I-4b** compared to **I-4a**. All these features make these materials promising for use as n-type OFET materials, with electron mobility of 0.10 $cm^2\ V^{-1}\ s^{-1}$. Zhang and co-workers reported two series of A–D–A–type OSC based isatin derivatives with a rigid indacenodithieno[3,2-b]thiophene moiety acting as a central bridge and both ends

capped with strong electron-withdrawing indole (**I–5a**) or pyrrolo[4,5-b]pyridin-2,3-dione (**I–5b**) [13]. The replacement of the benzene ring with a pyridine moiety enhances the planarity and improves the structural ordering through non-covalent interactions, due to the lower steric requirements of nitrogen atom compared to the C-H unit, which results in a remarkable enhancement of hole mobility. In a separate study, the same authors showed that changing the end group from the **I–5c** to the thienyl methylene-oxindole unit, **I–5d**, while keeping the same π–bridge, indacenodithieno[3,2-b]-thiophene, enables high hole OFET-mobility of over 0.27 cm^2 V^{-1} s^{-1} [14]. A series of A–D–A–type OSC based on indacenodithiophene as a bridging group were synthesized and their opto-electrical properties were investigated by Zhao [15, 16]. Compound **I–6a** in chloroform solution showed a major absorption peak at 540 nm, which underwent a considerable red-shift for **I–6b** (675 nm) and **I–7** (730 nm) because of the gradual increase in the electron-withdrawing ability of the acceptor moieties of these molecules. This red-shift was accompanied by reducing the corresponding optical band-gap values from 1.95 eV for **I–6a** to 1.48 eV for **I–6b** and 1.43 eV for **I–7**. The LUMO energy level of these A–D–A–type OSC was found to vary significantly with the strength of the acceptor fraction. The LUMO energy of **I–6b** was significantly reduced to −4.02 eV. On the other hand, the LUMO energy of **I–7** was close to that of **I–6b**.

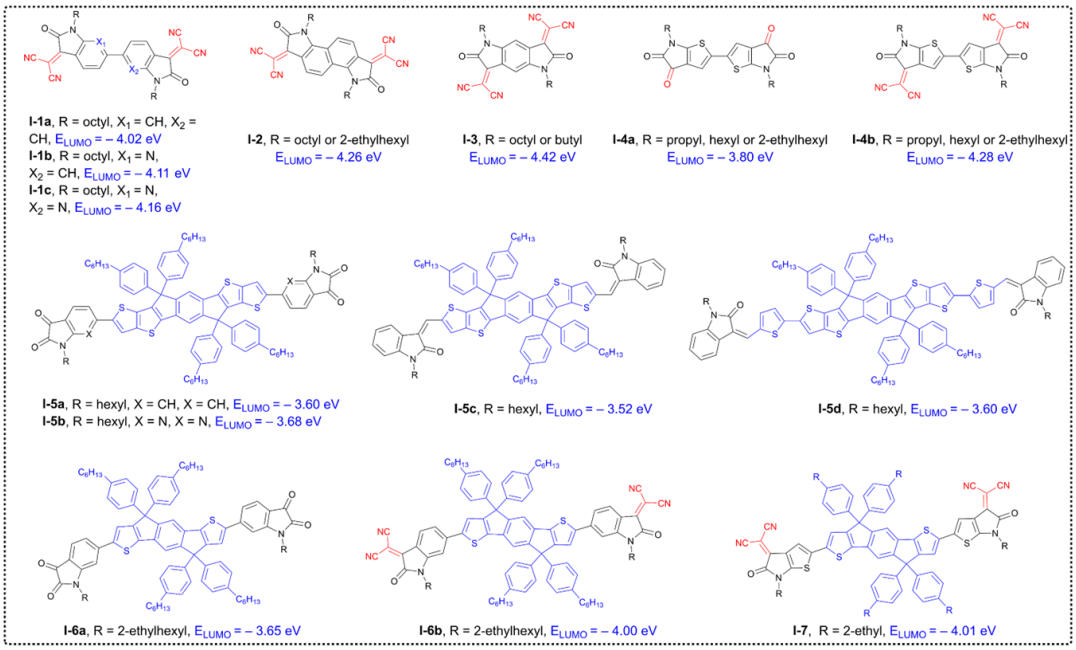

Figure 1 Chemical structures of bis-lactam-based organic materials reported in the literature.

Besides their use as OFET materials, A–D–A–type OSC with deep LUMO levels could be used as electron transporting materials for perovskite solar cells [17-19]. Recent works have shown that the energy level matching between the perovskite's conduction band and the electron-transporting materials' LUMO significantly impacts device performance by promoting electron extraction and inhibiting recombination between interfaces. When implemented in a perovskite solar cell, an acceptor material with a LUMO energy around -3.80 eV can facilitate electron transfer from the bottom of the perovskite conduction band to its LUMO level.

Despite these studies, there has been no systematic study on the effect of substitution positions and conjugation lengths of the bridging groups on the photophysical and the electrochemical properties of A–D–A–type OSC to understand the parameters required for ideal acceptor materials. We propose that modifying of π–linking units of A–D–A OSC would tune the energy levels and photophysical properties of resulting materials, since the π–bridge in the A–D–A OSC plays an

important role in regulating the absorption and charge carrier mobility.

Herein we present the design and synthesis of a new set of small molecules with A–D–A–type OSC architectures that consist of π–conjugated bridge with different π–spacer lengths as donor units and two isatylidene malononitrile segments as the terminal acceptor groups, Figure 2. Isatin moiety possess four positions available for introducing functional group. The 4 and 6 positions result in a linearly conjugated chromophore, while the substitutions at the 5 and 7 positions generate non-conjugated materials. The objective is to vary the conjugation length by different π–spacer groups, to alter the linkage position of the phenyl of the isatin core (4-position vs. 6-position), and to analyze how these modifications affect the photophysical, and electrochemical properties of these new dyes. DFT and TD–DFT studies have been performed to gain an insight into their electronic properties by determining the energy levels and maps of HOMO and LUMO as well as the HOMO–LUMO gap. To demonstrate their ability to act as n-type OSC, we performed SCLC measurements to probe their electron mobility. Electron only devices were fabricated by the spin-coating and the trap-limited electron mobility was calculated using Mott-Gurney law. **10a** exhibited an intrinsic moderate electron mobility of 8.94×10^{-4} cm^2 V^{-1} s^{-1}. The potential practical utility of these materials is demonstrated as an electron-transport materials (ETMs) for PSCs, with maximum power conversion efficiencies of 6.24% and 6.94% for **10a** and **4/10a** respectively.

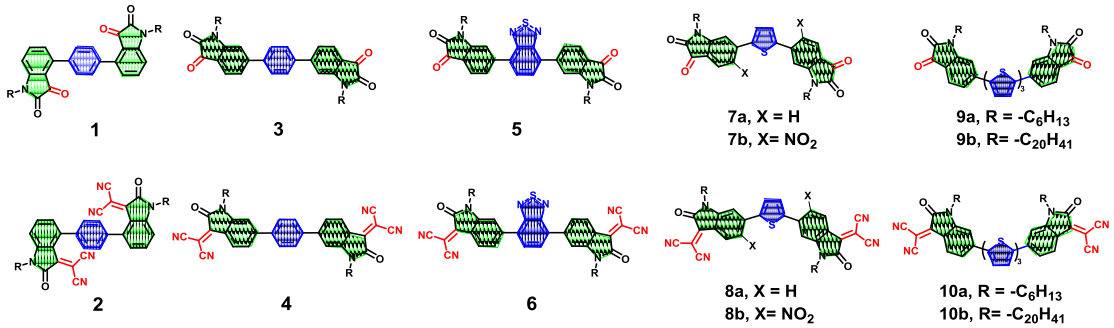

Figure 2 Chemical structures of bis-isatin and di-2-(2-oxindolin-3-ylidene) malononitrile derivatives.

2. Experimental section

2.1 Materials and methods

Detailed synthetic procedures and characterization, NMR, UV–visible spectroscopy and high-resolution mass spectroscopy of new molecules, their intermediates, device fabrication and current-voltage characteristics, are available in the supplementary information (SI).

2.2 Theoretical and computational details

Geometries of all the molecules were fully optimized with B3LYP functional and 6-31G(d) basis set with the Polarizable Continuum Model (PCM) using the integral equation formalism variant (IEFPCM) in tetrahydrofuran solvent (THF, ε=7.4257) [B3LYP/6-31G(d)/THF] [20, 21]. The hexyl substituents on the N atoms of the isatylidene segments were replaced with ethyl to reduce calculation cost. Frequency calculations were performed to confirm the optimized geometries to be true energy minimum. On the basis of the optimized geometries at B3LYP/6-31G(d)/THF level, molecular orbital energies and electron energies were then calculated with M06L functional and 6-31G(d) basis set with IEFPCM solvent model in THF [M06L/6-31G(d)/THF]. Electronic absorption spectra were simulated based on the

excited state data calculated with TD-DFT method at M06L/6-31G(d)/THF level using B3LYP/6-31G(d)/THF geometries. All calculations were carried out using the Gaussian 16 program [22, 23].

3. Results and discussion

3.1 Design, synthesis and characterization of A–D–A–type OSC

The synthetic route to the target A–D–A–type OSC based on isatin derivatives, is shown in Scheme 1. The detailed synthesis and characterization are shown in the Experimental Section of SI. The desired bromoisatins (**13**, **14**) were synthesized through a two-step procedure followed by intermediate **12**, using the corresponding commercial 3-bromoaniline, **11**, as a starting material. To overcome the solubility issue, alkyl solubilizing side chains, hexyl or long branched alkyl were introduced to **13** or **14** at the nitrogen atom to produce **16** or **17a–c** in excellent yields. **16** and **17a** were further reacted with 1,4-benzenediboronic acid bis(pinacol) ester, in the presence of $[Pd_2(dba)_3]$ as a catalyst, and K_3PO_4 as a base to afford **1** and **3** in 60% and 70% yield, respectively. Subsequently, the bis-isatin compounds **1** and **3** were treated with malononitrile via a Knoevenagel condensation reaction to generate the target products **2** and **4**, respectively. Replacement of phenyl with electron-withdrawing benzo[c][1,2,5]thiadiazole (BTD) was targeted to analyze the effect of π–bridge. The Suzuki-Miyaura reaction of **17a** with BTD afforded **5** with 55% yield and subsequent Knoevenagel condensation with malononitrile provided **6** with 80% yield. Introducing a thiophene ring between the acceptor units was realized under Stille coupling reaction between **17a** and 2,5-di-tributylstannylthiophene in the presence of

[Pd(dppf)Cl_2] as a catalyst and afforded **7a** in 64% yield. With the aid of a catalytic amount of the pyridine, the Knoevenagel condensation reaction could occur at room temperature, and afforded **8a** in 89% of yield. It was envisaged that introduction of a nitro group, which could be subsequently employed in a late-stage in a double Cadogan cyclisation, would be the optimal strategy to prepare five rings fused systems Y6 analog. The dinitro derivatives **7b** and **8b** were obtained using Stille coupling reaction followed by a Knoevenagel condensation with malononitrile. To extend the conjugation length between the two isatin moieties, terthiophene was appended to the isatin. Reaction of 2-tributylstannylthiophene with **17a** or **17b** under Stille coupling condition, produced the asymmetrical dye **18a** (or **18b**) in 80% yield. Selective bromination at the 5-position of thiophene using the N-bromosuccinimide, afforded the intermediate **19a** (or **19b**). The obtained bromo thienyl-isatin was then coupled to the 2,5-di-tributylstannylthiophene to form **9a**. To improve the solubility, the analogue **9b** with a branched alkyl chain was obtained in a similar yield.

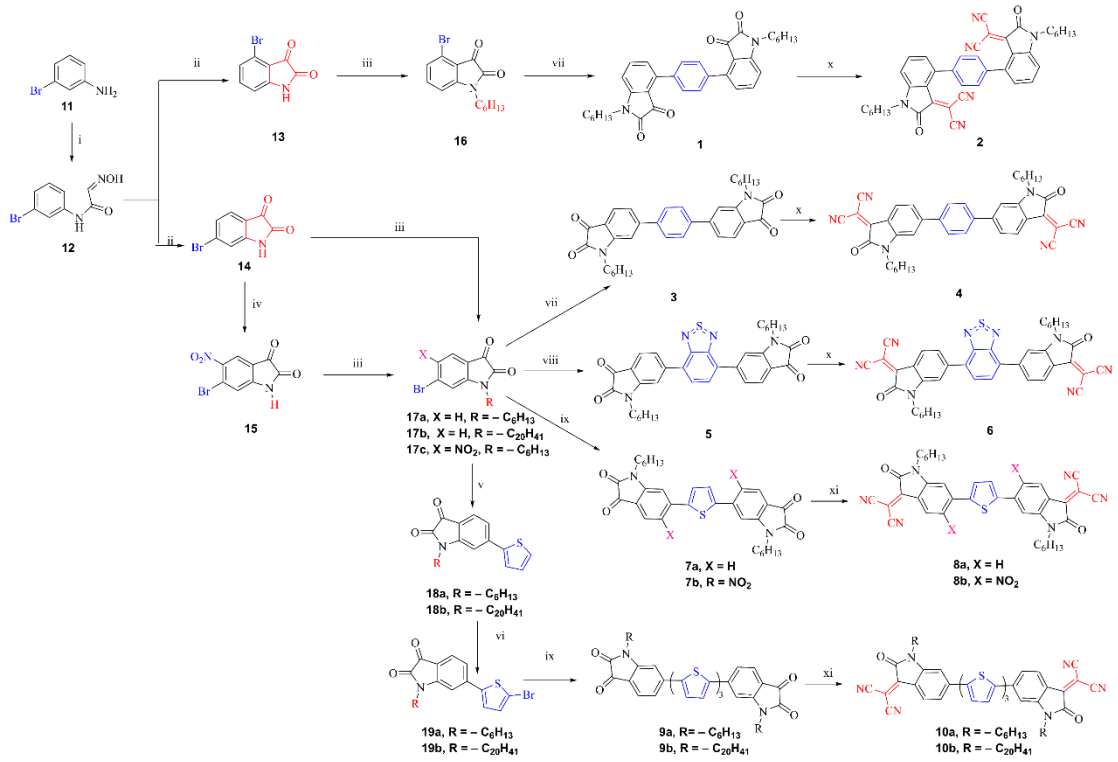

Scheme 1 Synthetic route to bis-isatin compounds **1**, **3**, **5**, **7**, **9** and di-2-(2-oxindolin-3-ylidene) malononitrile derivatives **2**, **4**, **6**, **8**, **10**. Reagents and conditions: (i) chloral hydrate, Na_2SO_4, $H_2NOH{\cdot}HCl$, 65 °C, 2 h; (ii) H_2SO_4, 75 °C, 15 mins, 35% over two steps; (iii) K_2CO_3, Br-R, R = $-C_6H_{13}$ or $-C_{20}H_{41}$, DMF, 90 °C, 24 h, 80%-90%; (iv) $NaNO_3$, H_2SO_4, 0 °C, 1 h, 87%; (v) 2-tributylstannylthiophene, [Pd(dppf)Cl_2], DMF, 90 °C, 80%; (vi) AcOH, NBS, THF, 0 °C, 5 h, 82%; (vii) 4,4,5,5-tetramethyl-2-(4-(4,4,5,5-tetramethyl-1,3-dioxolan-2-yl)phenyl)-1,3,2-dioxaborolane, P(o-tyl)$_3$, [$Pd_2(dba)_3$], K_3PO_4, Toluene, H_2O, 90 °C, 24 h, 60%-70%; (viii) [$Pd_2(dba)_3$], 4-(4,4,5,5-tetramethyl-1,3,2-dioxaborolan-2-yl)-7-(4,4,5,5-tetramethyl-1,3-dioxolan-2-yl) benzo[c][1,2,5]thiadiazole, P(o-tyl)$_3$, K_3PO_4, toluene, H_2O, 90 °C, 24 h, 55%; (ix) 2,5-di-tributylstannylthiophene, [Pd(dppf)Cl_2], DMF, 90 °C, 64%-75%; (x) malononitrile, EtOH, reflux, 80%-90%; (xi) malononitrile, pyridine, EtOH, rt, 85-90%.

All the newly prepared A–D–A–type OSC based on isatin were fully characterized by ^{1}H NMR, ^{13}C NMR spectroscopy and high-resolution mass spectrometry. For instance, Figure 3 provides an example of how the ^{1}H NMR spectra of A–D–A–type OSC compound **5** and its malononitrile homologue **6** variants. The ^{1}H NMR spectrum clearly display two doublets and two singlet peaks in the aromatic region, plus one at 3.80 ppm belonging to N-CH_2, agreeing well with its chemical structure and chemical environment. After the Knoevenagel condensation reaction, the signal of Ha' of **5**

shifted from 7.78 to 8.29 ppm (Ha in **6**). The Ha proton produces the most downfield signal owing to the large deshielding effect of the neighboring-CN moiety (hydrogen bonding). Nevertheless, no chemical shifts were observed for the other three peaks after the condensation reaction.

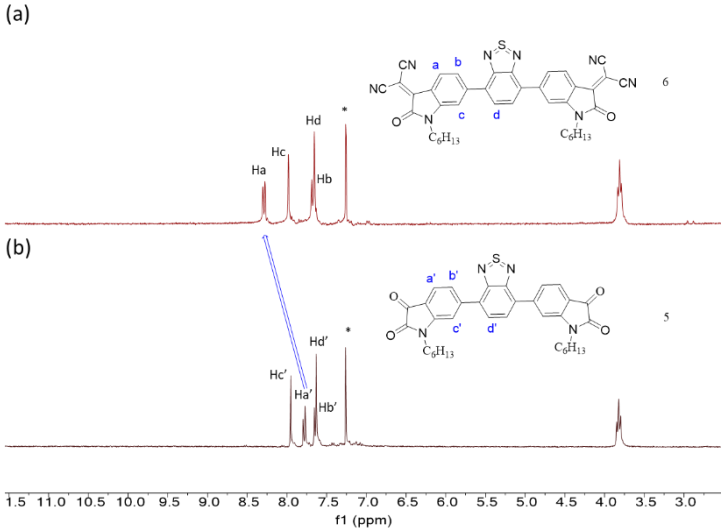

Figure 3 ^{1}H NMR spectra of compounds **6** (a); and **5** (b) in $CDCl_3$ (*: solvent peak).

3.2 Optical characterization

The photophysical properties of A–D–A–type OSC based on bis-isatin and di-2-(2-oxindolin-3-ylidene) malononitrile derivatives were investigated by UV–vis spectroscopy, and the corresponding absorption data were listed in Table 1. For comparison purposes between malononitrile derivatives and bis-isatin derivatives, the absorption spectra of **1**, **3**, **5**, **7a, 7b, 9a** and their derivatives, **2**, **4**, **6**, **8a**, **8b, 10**, were normalized to enable direct comparison of substituent effects, Figure 4. We note that we encountered difficulties in reproducibility of the molar extinction coefficients, because these molecules exhibit a strong tendency to aggregate in dilute solution. Their spectra shared a common feature with two absorption bands: a low energy band in the visible region attributed to the ICT transition arising from the acceptor moieties

and a high energy band in the range of 300–450 nm attributed to the π–π* bridge. The position of these bands were strongly influenced by the molecular structure of compounds, conjugation length of π–bridge, and the nature of acceptor moiety. The effect of the acceptor end group was demonstrated by comparing the absorption maxima of **7a** and **8a**, the solution spectrum of **8a** exhibits bands for the π→π* transition (457 nm) and ICT (550 nm), while those of **7a** are at 393 nm and 440 nm, demonstrating that the introduction of the dicyanovinylene groups resulted in a 100 nm bathochromic shift in absorption, (Table 1, entries 7 and 8).

A comparison of the absorption spectra of **3** (λ_{max} = 349 nm) with **7a** (λ_{max} = 393 nm) revealed that the replacement of phenyl with thienyl ring caused a red-shift of the high energy band. This observation clearly indicated that the incorporation of thiophene moiety in A–D–A–type OSC enhanced their ICT-properties, as previously reported in the literature [24, 25]. This trend was also observed for the malononitrile derivatives, where a bathochromic shift of 43 nm was seen for the high energy band. As shown in Figure S1 b, both absorption spectra of **1** and **3** exhibit two peaks assigned to π→π* transition (350 nm) and ICT (450 nm). A Comparison of the spectra of compounds **1** and **3** shows an increase of ICT band intensity for compound **1**. The enhancement of the ICT band intensity could be attributed to a better planarity of the structure induced by an electrostatic interaction between the carbonyl of isatin and the phenyl ring forming a hydrogen bond. However, there was no much variation between the main absorption peaks of the phenyl ring units at the 4- and 6- positions (compound **2** and **4**), Figure S1 c, probably because they are both linearly conjugated.

This is supported by geometry optimizations where the molecule **1** exhibits a more coplanar molecular conformation with a dihedral angle of 46 ° (Figure S2), while the dicyanovinyl analog **2** exhibits a 68° dihedral angle between the phenyl and isatin planes in its most stable conformation. The H-bond H···O distance of 2.60 A which is significantly shorter than the sum of van der Waals radii of O and H atoms (2.72Å) [26].Additionally, the possible steric hindrance of the chemical structure has always limited the introduction of a large aromatic ring at 4- position of isatin. The absorption spectra of **10a** and **10b** (Figure S1 d) showed almost identical absorptions in the visible range, indicating that changes in the alkyl group on the nitrogen atom hardly influenced the electronic structure of the malononitrile derivatives. For both series of bis-isatin and malononitrile derivatives, the absorption spectra revealed that the absorption peaks rising from the aromatic bridges were gradually red-shifted to longer wavelengths with increasing the conjugation length. For instance, **10a** exhibited a broad and strong absorption spectrum with a λ_{max} of 605 nm. Obviously, this red-shift could be attributed to the extended π–conjugation length compared with that of **8a**. Variation of the π–conjugated bridge units had a notable impact on the absorption profiles of the new bis-isatin and malononitrile derivatives. An intriguing feature observed was that **8b** displayed a blue-shift of the maximum of the absorption compared to **8a** (Figure 4b purple line vs. green line). This blue-shift could be attributed to the steric hindrance of the two nitro groups (-NO_2). This is consistent with studies by Jean at al. who reported the decrease intensities and hypsochromic shifts in the absorption spectra of non-coplanar conjugated molecules sterically

hindered by the bulky nitro group, such 2,2',4,4'-tetra-nitro-5,5'-dimethyl-3,3'-bithienyl; 3,3'-dinitro-5,5'-diacetyl-2,2'-bithienyl; and 3,3'-Dinitro-5,5'-dicarbometh-oxy-2,2'-bithienyl, are a result of the steric hinderance on the part of the ortho substituted groups [27]. A similar trend in the absorption features is observed when comparing the absorption bands, λ_{max} of **7a** and **7b**. The optical gaps of the bis-isatin derivatives were approximately 2.25 eV, while the optical gaps of the di-2-(2-oxindolin-3-ylidene) malononitrile series were lowered to around 1.90 eV, with the lowest optical gap of 1.63 eV for compound **10**.

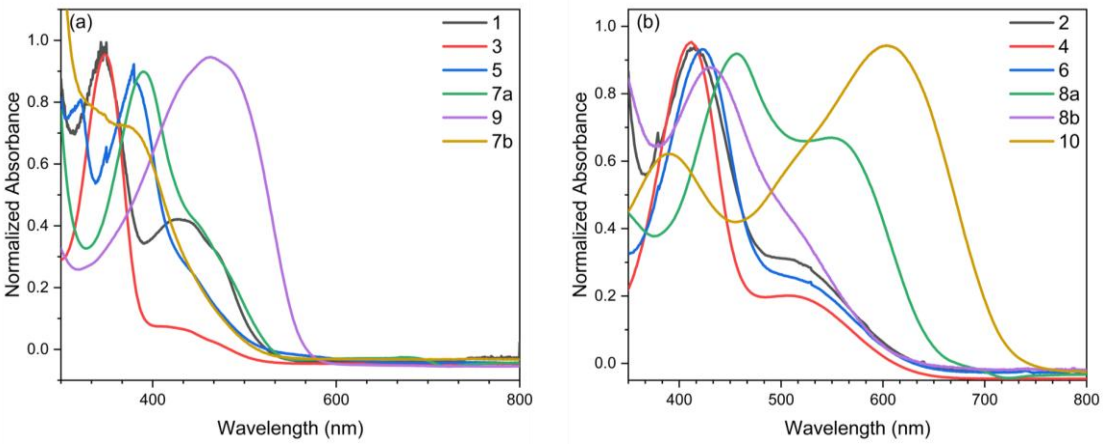

Figure 4 Normalized UV-vis absorption spectra of bis-isatin derivatives **1**, **3,** **5**, **7a**, **9a**,**b** (a) ; and di-2-(2-oxindolin-3-ylidene) malononitrile derivatives **2**, **4**, **6**, **8a**, **8b**, **10a**,**b** (b) in THF (concentration range 0.05–0.10 mg/ml).

Compounds	$\lambda_{max}{}^{sol}$ (nm)[a]	$\lambda_{onset}{}^{sol}$ (nm)[a]	$E_g{}^{opt}$ (eV)[b]
1	430, 347	530	2.34
2	514, 415	628	1.97
3	434, 349	532	2.33
4	515, 414	630	1.97
5	440, 380	546	2.27
6	533, 423	651	1.90
7a	440, 393	553	2.24
8a	550, 457	670	1.85
8b	432, 520	642	1.93

9a,b	462	586	2.11
10a,b	605, 383	758	1.63

Table 1 Optical properties analysis data of synthesized bis-isatin and di-2-(2-oxindolin-3-ylidene) malononitrile derivatives **1**–**10**. [a]λ_{max} in THF solution, [b]the optical energy gap is estimated from the absorption onset in THF solution $E_g^{opt} = 1240 / \lambda_{onset}$.

3.3 Electrochemical study

The electrochemical behavior of the A–D–A type OSC based on bis-isatin and malononitrile derivatives were evaluated by means of CV using tetrabutylammonium perchlorate as supporting electrolyte in dichloromethane and the electrochemical data were listed in Table 2. The energy levels of HOMO (E_{HOMO}) and LUMO (E_{LUMO}) were respectively estimated from the onset potential of the first oxidation and reduction peak vs. Fc/Fc^+, assuming an ionization energy of 4.80 eV for ferrocene. The CVs of the bis-isatin derivatives showed one oxidation wave and two well-reversible reduction waves. The reduction potentials were found to be dependent on the bis-isatin structure. The CV of di-2-(2-oxindolin-3-ylidene) malononitrile derivatives under the same condition also showed two sets of reduction, but shifted to more positive values than that of the parent compound, bis-isatin, Figure 5. For example, compound **2** exhibited E_{red1} = –0.61 V (vs Ag/AgCl) compared to **1** (–1.11 V), thus leading to a shift of 0.50 V. This suggests that the LUMO energy levels were predominantly controlled by the nature of the acceptor units. Regardless of the nature of the end-group substituents, both reduction potentials followed the trend Ph < BTD < Th. For instance, in the first reduction process of the A–D–A–type malononitrile family, the BTD and thiophene were easier to reduce than the phenyl, corresponding to peaks of –0.52 V, –0.46 V, and –0.58 V respectively. Nevertheless, the difference in

the reduction potential was less than 0.15 V, this small change was indicative of a minor contribution of the flanking aryl groups to the LUMO (Figure 5). On the other hand, compounds **7a** and **9a**, **b** (or compounds **8a** and **10a**, **b**) with one thiophene and terthiophene unit as a π–bridge group presented pretty close LUMO energy levels. Changing the conjugate length of the π–bridge had a more significant effect on the HOMO energy level. **8b** functionalized with -NO_2 and -CN group exhibited a low-lying LUMO energy level. The LUMO energy level could be tuned from –3.54 eV (**7a**) to –4.23 eV (**8b**), due to the fact that nitro was one of the strong electron-accepting groups.

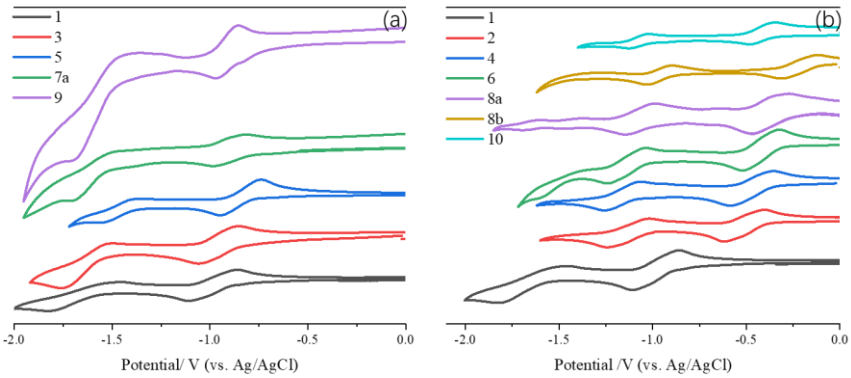

Figure 5 Cyclic voltammograms of bis-isatin compounds **1**, **3, 5**, **7a**, **9a**, **b** (a); and malononitrile derivatives **2**, **4, 6**, **8a**, **8b**, **10a**, **b** (b) in dichloromethane (concentration range of 10^{-4} to 10^{-3} M).

As shown in Table 2, the LUMO energy levels of A–D–A type OSC based on di-2-(2-oxindolin-3-ylidene) malononitrile derivatives (~ –4.0 eV) located lower than those of bis-isatin derivatives, where values around –3.50 eV were measured. This is in accordance with the fact that the strong electron-withdrawing ability of the dicyanovinylene group strongly affects the LUMO energies. The HOMO levels of bis-isatin and di-2-(2-oxindolin-3-ylidene) malononitrile derivatives were estimated to be slightly above –5.50 and −5.80 eV, respectively (except compound **8b**, **9**, **10**).

Changing the linkage pattern of the malononitrile derivatives (4-position to 6-position) had a small effect on the HOMO and LUMO energy levels, with a slightly higher HOMO energy level of 0.05 eV and a slightly lower LUMO energy level of approximately 0.02 eV for **4** compared to that of **2**. The HOMO energy level of **8a** was 0.07 eV higher than that of **4**, which was caused by the stronger electron-donating ability of thiophene. In addition, the HOMO energy level of **7a** was significantly higher than that of **5** (–5.35 vs. –5.53 eV, Table 2) in bis-isatin series, which also indicated the strong electron donor characteristics of the thiophene. The HOMO level of compound **10** bearing either linear or branched alkyl side chains (**10a** or **10b**) was much higher than one thiophene or one phenyl unit bridge compound, due to the nature of the long conjugation donor chain. The resulted HOMO–LUMO gaps decreased to 1.20 eV. Finally, a change in the alkyl chain length does not affect the UV-visible and the electrochemical properties, both series, 10a, 10b exhibit identical HOMO/LUMO energy levels, suggesting that the influence of the alkyl chains on the HOMO/LUMO energy level is negligible.

	E_{red1} (eV)	E_{red}^{onset} (eV)	E_{LUMO} (eV)[c]	E_{HOMO} (eV)[c]	E_g^{CV} (eV)[d]
1	–1.11	–0.87	–3.40	–5.46	2.06
2	–0.61	–0.36	–3.91	–5.92	2.01
3	–1.03	–0.81	–3.46	–5.52	2.06
4	–0.58	–0.34	–3.93	–5.87	1.94
5	–0.93	–0.74	–3.53	–5.53	2.00
6	–0.52	–0.29	–3.98	–5.82	1.84
7a	–0.94	–0.73	–3.54	–5.35	1.81
8a	–0.46	–0.19	–4.08	–5.80	1.88
8b	–0.30	–0.04	–4.23	–5.96	1.73
9a,b	–0.95	–0.71	–3.56	–5.11	1.55
10a,b	–0.47	–0.24	–4.03	–5.23	1.20

Table 2 Cyclic voltammetry results of bis-isatin and di-2-(2-oxindolin-3-ylidene) malononitrile derivatives **1-10**. [c]HOMO/LUMO energy levels were calculated from the onset of oxidation and reduction waves using an offset of −4.80 eV for saturated Ag/AgCl, E_{LUMO} = –4.80 eV – [(Eredonset) – $E_{1/2}$(ferrocene)] and E_{HOMO} = –4.80 eV – [(E_{ox}^{onset}) – $E_{1/2}$(ferrocene)], [d]E_g^{cv}= electrochemical gap.

3.4 Theoretical studies

3.4.1 Molecular orbitals

Figure S3 in SI shows the molecular orbital maps of all the molecules. Both HOMO and LUMO are fully delocalized on the two di-2-(2-oxindolin-3-ylidene) malononitrile terminal acceptor groups and the π–conjugated bridge donor segments. The HOMOs mainly occupy the double bonds along the long-axis direction of the molecules while the LUMOs mostly distribute on single bonds perpendicular to the long-axis direction. For bis-isatin compounds, the distribution of HOMO and LUMO decreases from center π–bridge to terminal A segments. On the contrary, the HOMO and LUMO of malononitrile derivatives appear to distribute more on acceptor than π–bridge. Table 3 summarized the calculated HOMO and LUMO energy levels. For bis-isatin compounds, the HOMO energies have the order of **4** ≈ **6** < **8a** < **10a** while the LUMO energies show the trend of **6** < **8a** < **4** ≈ **10a** (Table 3). The resulted HOMO–LUMO gaps decrease in the order of **4** > **6** > **8a** > **10a**. It is a common rule that both HOMO and LUMO increase with polymer/oligomer length and the relatively higher HOMO and LUMO energy of **10a** than **8a** are easily understandable. The higher HOMO and LUMO energy of **8a** than **6** indicates that thiophene moiety has larger electron-donating ability than BTD group.

	$E_{g\text{-}opt}^{DFT}$	E_{LUMO}^{DFT}	E_{HOMO}^{DFT}	E_g^{DFT}
1	2.30	–3.37	–5.60	2.23
2	1.83	–4.01	–5.78	1.77
3	2.35	–3.48	–5.68	2.20
4	1.78	–4.13	–5.76	1.63
5	2.17	–3.67	–5.69	2.02
6	1.72	–4.20	–5.76	1.56
7a	2.17	–3.60	–5.54	1.94
8a	1.62	–4.21	–5.62	1.41
8b	1.78	–4.46	–6.06	1.60
9a,b	1.68	–3.48	–5.00	1.52

10a,b	1.30	–4.05	–5.12	1.07

Table 3 Calculated energies of the HOMO and the LUMO (E_{HOMO}^{DFT} and $E_{LUMO}^{DFT)}$, HOMO–LUMO energy gap (E_g^{DFT}), optical gap ($E_{g\text{-}opt}^{DFT}$, excitation energy of the first excited state), at M06L/6-31G(d) level with IEFPCM solvent model in THF on the basis of the optimized geometries at B3LYP/6-31G(d) level with IEFPCM solvent model in THF. All energies are in eV.

Figure 6 reports a survey of the calculated orbital energy levels and maps of the frontier molecular orbitals of bis-isatin and di-2-(2-oxindolin-3-ylidene) malononitrile derivatives. The higher energy levels of HOMO and LUMO of **2** than **4** may be due to the larger steric hindrance between the phenyl ring and dicyano methylene group of isatin moiety in **2** than in **4**. Substituting one carbonyl function of isatin moiety with stronger electron-accepting dicyano methyelene $C(CN)_2$ in malononitrile derivatives largely decrease both the HOMO and LUMO energies and results in significantly smaller HOMO–LUMO gap (Figure 6). Compound **8b** shows lower HOMO and LUMO energy than **8a** due to the introduced electron-withdrawing-NO_2 group. However, different from the fact that strong electron-accepting $C(CN)_2$ in malononitrile derivatives reduces the LUMO energy more significantly than the HOMO and thus induces decreased optical band-gap, the nitro group in **8b** reduces the HOMO energy more significantly than LUMO energy and results in larger HOMO–LUMO gap for **8b** than **8a**.

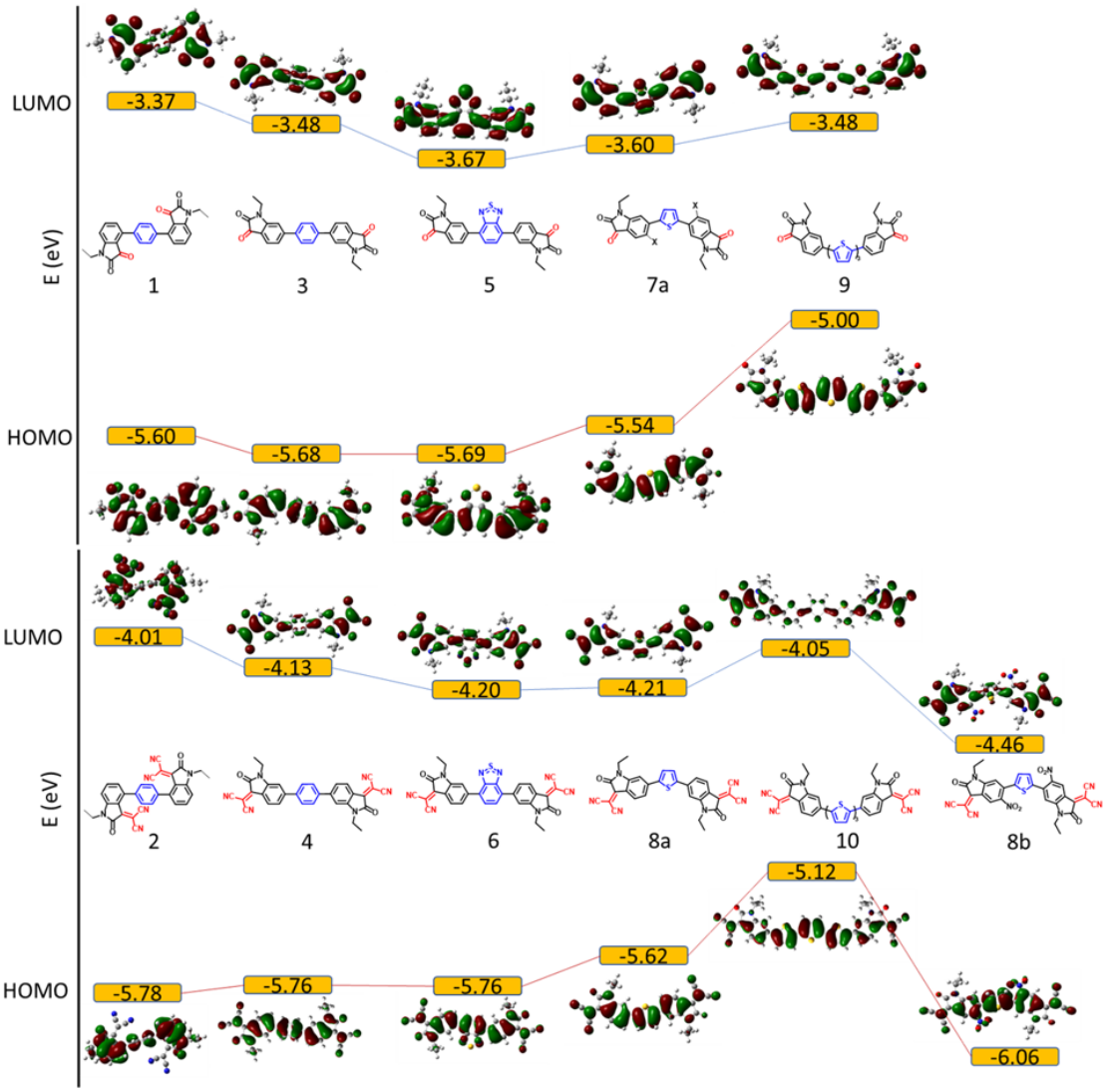

Figure 6 The evolution of energy levels of frontier molecular orbitals of five bis-isatin derivatives (top); and six di-2-(2-oxindolin-3-ylidene) malononitrile derivatives (bottom). Lines connecting the dots (different compounds) to better visualise the trends.

3.4.2 Electronic transitions

The computed energy levels are close to those obtained experimentally in the THF solution, indicating that M06L provides a good estimate of the HOMO–LUMO gap. The aforementioned changes in the orbitals' shapes and energies can be related to the differences in the electronic transitions involved in the lowest-energy and highest-energy excited states of these molecules. The calculated optical gap (excitation energy of the first excited state) has the same trend as the HOMO–LUMO

gaps, but the optical gaps have larger values due to orbital coupling energy. The lowest energy bands are due to the electronic transition from HOMO to LUMO and could be assigned to ICT transition between the π–conjugated bridge and end-group acceptor. ICT type transitions generally have a weak intensity, however, when the π–conjugation length increases, the intensity of the lowest energy band increases due to the contribution from π–π* transition of the donor. The comparison between the calculated and experimental HOMO and LUMO energies and HOMO–LUMO gap of all the molecules is depicted in Figure 7. The calculated energy values of HOMO and LUMO agree with experimental data within less than 0.15 eV for the entire series of molecules, which is not the case for the optical band gap energy. The underestimation is more severe for the larger molecules **9** and **10**. The error, however, is not dramatic considering the size of the molecules. The high energy band is attributed to the π–π* transition for both π–bridge and acceptor groups.

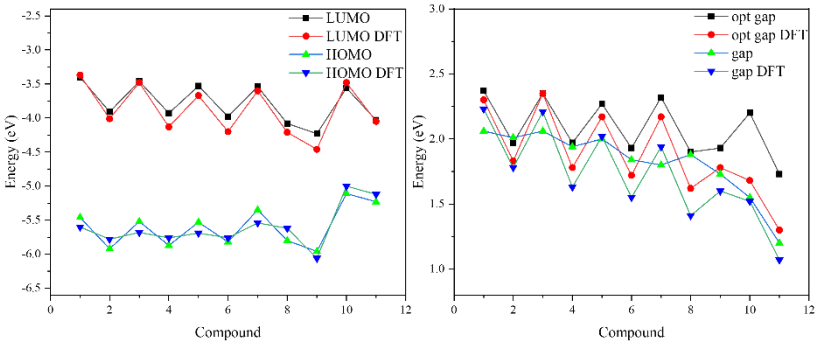

Figure 7 Comparison between calculated and experimental LUMO, HOMO, HOMO–LUMO energy gap and optical band gap of eleven bis-isatin and di-2-(2-oxindolin-3-ylidene) malononitrile derivatives.

DFT simulated UV–vis data, Figure 8 supports the above observations that these lower energy transitions which are assigned as ICT have the maximum contribution in the visible region. In short summary, TD–DFT calculations were carried out to

investigate the electronic effects of conjugation length and the substitution position of the end-group on molecular orbitals and electronic absorption spectra. The calculated molecular orbital energies and gap correspond well with the corresponding experimental data. The deviation between calculated and experimental orbital energies are less than 0.15 eV for most cases. In addition, the calculated trends for orbital energies among different compounds are the same as the experimental ones, as shown in Figure 7.

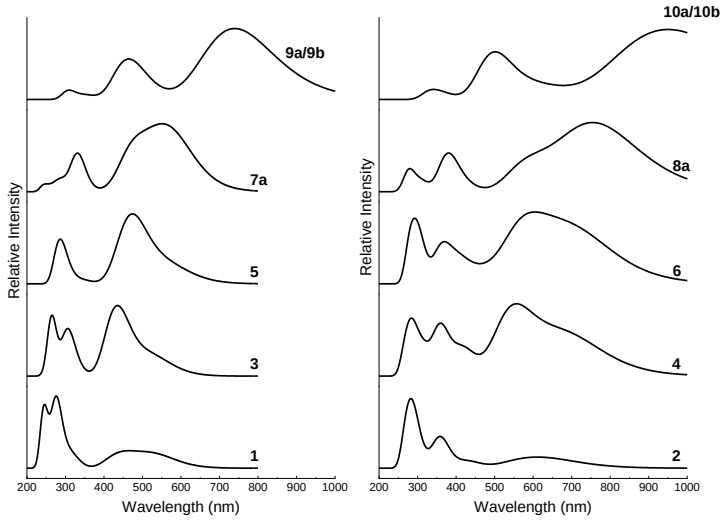

Figure 8 TD–DFT simulated UV/vis absorption spectra with half-width at half height of 2000 nm of the bis-isatin and di-2-(2-oxindolin-3-ylidene) malononitrile derivatives.

3.5 Electrical characterization

Further electronic characterization has been performed by investigating electron transport ability of these materials. In order to assess their inherent charge transport properties, the electron mobility of **4** and **10a**, that differ by the length of the π‑bridge between the malononitrile centers, were measured by the SCLC method and compared with those reported in the literature. The following specified configurations were utilized for the electron-only device: ITO/SnO_2/active layer (**10a** or **4**)/LiF/Al. As shown in Fig. 9, the **10a** or **4** molecule-based devices exhibited an SCLC behavior

with a clear slope variation from 4–10 V. From these *J-V* curves, the charge carrier mobility can be extracted using the Mott-Gurney equation: "$J_{SCLC} = \frac{9}{8}\frac{\varepsilon_0 \epsilon_r}{L^3}\mu V^2$". Therein ε_0, is the permittivity of vacuum, ε_r is the relative permittivity of the organic compound, μ is the charge carrier mobility, V is the voltage, and L is the thickness of the tested layer. As plotted in Figure 9, the current density-voltage characteristic curves and SCLC fittings for both films reveal the SCLC region (> 6V). This allows us to extract an average electron mobility of $\mu_e = 3.51\times10^{-4}$ cm^2 V^{-1} s^{-1} and $\mu_e = 3.61\times10^{-5}$ cm^2 V^{-1} s^{-1} for **10a** and **4** respectively. The highest electron mobility of **10a** is 8.94×10^{-4} cm^2 V^{-1} s^{-1}. When compared to other A–D–A–type OSC small molecules from the literature, the mobility of **10a** and **4** are in the same order of magnitude, where bis-lactam-based materials had an OFET mobility of 2.30×10^{-4} cm^2 V^{-1} s^{-1}.[28]

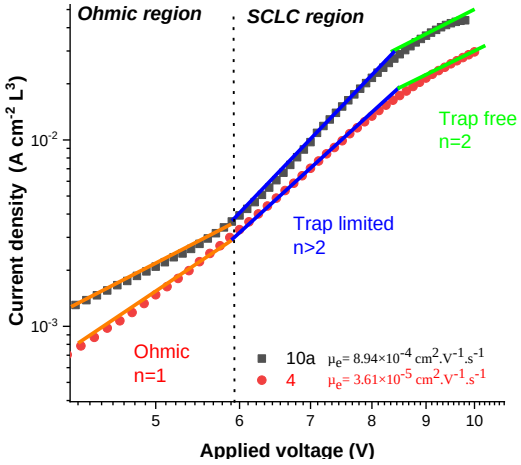

Figure 9 SCLC measurements of the electron-only devices for **10a** and **4** semiconductors with ohmic and trap-free space charge limited current regions.

Based on these results, several observations can be drawn. First, the finding that the higher mobility observed in films of **10a** (A–D–A) cannot be explained only by the downshifted LUMO energy level, from –3.93 eV for **4** to –4.03 eV for **10a**, which could, in fact facilitate electron injection, but also by a better planarity of **10a** compared to **4**. In fact, a better coplanarity of the π–system due to the introduction of

thiophene units, may induce a strong π–π stacking interactions in the solid state, leading to improved charge transport and higher electron mobility value. Second, the finding that the electron mobility of **4** is only one order of magnitude lower than the electron mobility of **10a** means that the molecular design, extending π–conjugation core, does not affect too much the electrical properties. As reported in literature charge transport, morphology and molecular aggregation in thin film are intimately related. Surface morphologies of **10a** and **4** films were examined by atomic force microscopy (AFM). As shown in Figure 10 both films exhibited a relatively smooth surface with root mean square of 0.96 nm for molecule **4**, and 1.15 nm for molecule **10a**, indicating their good film forming ability and more uniform thin film microstructures.

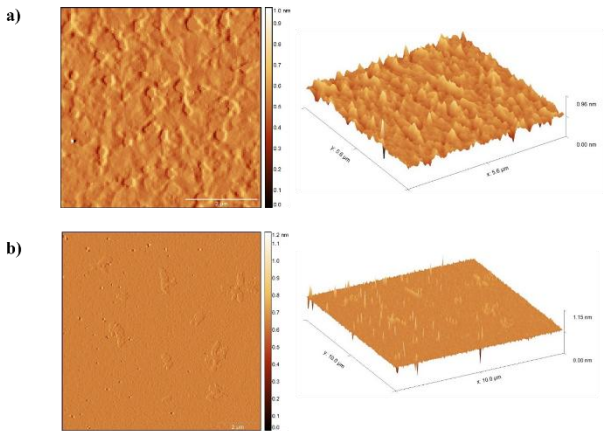

Figure 10 AFM topographic images of a) **4** and b) **10a** thin film on silicon wafer.

3.6 Photovoltaic properties

To demonstrate the functionality of the new acceptor materials as an active layer in optoelectronic devices, we implemented them as electron-transport layer (ETL) in perovskite solar cells with the configuration ITO/PEDOT:PSS/triple cation perovskite/ ETM/BCP/Ag (ETM: PCBM or **10a**) with a 7 nm of bathocuproine (BCP)

as a hole blocking layer in the ETL/Ag interface, Figure 11. We chose **10a** since it has a suitable LUMO energy level of –4.03 eV as that of PCBM (–4.20 eV), which lies well below the conduction band edge of triple cation perovskite, facilitating efficient charge extraction from the perovskite to the ETL, and also has a good electron mobility.

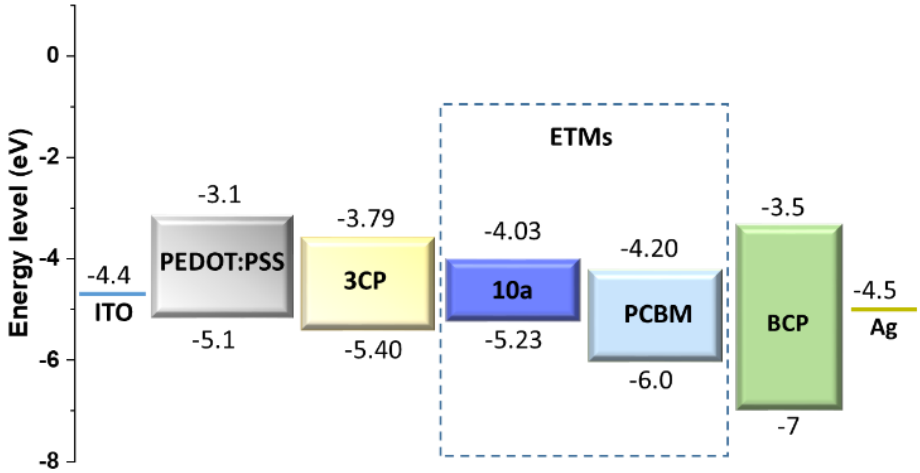

Figure 11 Energy band diagram of malononitrile derivative **10a** material used as an ETM in the perovskite solar cell.

The **10a** solutions were optimized to a concentration of 5 mg/ml and tested for different spin coating deposition speeds. Figure 12 shows the *J*–*V* curve of champion devices with **10a**, **4**/**10a**, and PCBM as an ETM, respectively. Table 4 summarizes the corresponding PV parameters.

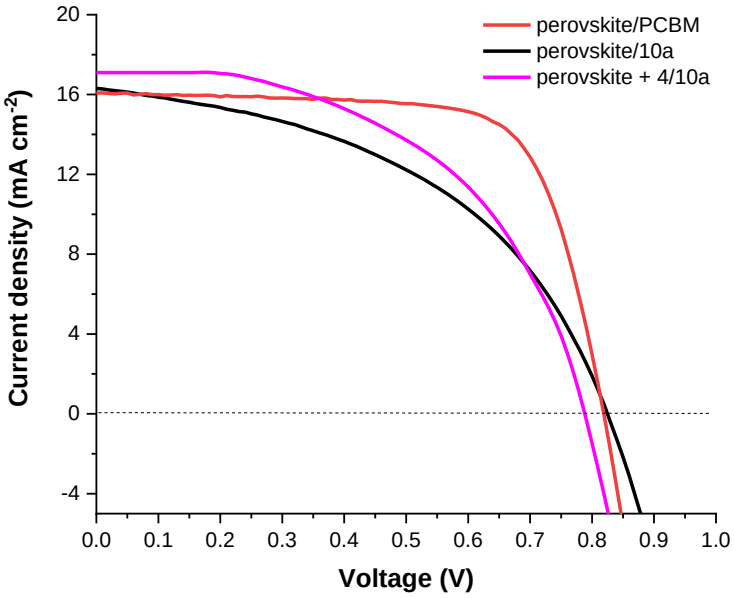

Figure 12 *J–V* characteristics of solar cells employing **10a** (black), **4** (passive tretment)/**10a** (pink) and PCBM (red) as ETL and triple cation perovskite FA0.85Cs0.15Pb(I0.8Br0.2)3 as absorbing layer.

ETM	J_{sc} [mA cm^{-2}]	V_{oc} [V]	FF [%]	PCE [%]
PCBM	16.70	0.81	73	9.44
	(15.85)	(0.80)	(72)	(9.05)
10a	16.30	0.82	47	6.24
	(14.50)	(0.78)	(46)	(5.34)
4/10a	17.11	0.79	51	6.94
	(17.53)	(0.81)	(50)	(6.78)

Table 4 PV parameters of PSCs using PCBM or **10a**, **4** (passive tretment)/**10a** and PCBM as ETMs. Data in parenthesis are the average over 8 for PCBM, 6 for **10a** and 5 for **4** /**10a**.

The surface morphology of perovskite layer was examined by SEM and AFM (top-view SEM in Figure 13 and AFM images in Figure S3 in SI). The distribution of grain sizes seems more homogeneous for the perovskite film cast on ITO/PEDOT:PSS and exhibits large grains size of between 400–500 nm range (Figure 13a). Figure 13b displays cross-sectional SEM image of the completed device (ITO/PEDOT:PSS/perovskite/**10a**/BCP/Ag), and shows the film thicknesses and morphologies of each layer. Thus, it can be seen that a 680 nm thick perovskite layer having a smooth and flat surface is in intimate contact with the **10a** layer of 55 nm

and BCP of 5 nm thickness. An almost 100 nm thick of ITO/PEDOT:PSS layers (the PEDOT:PSS layer is not very recognizable) is in close contact with the perovskite layer, without defects at the interface. As per literature reports, device architecture (p-i-n), employing PCBM as ETL, ITO/PEDOT:PSS/triple-cation perovskite/PCBM/ BCP/Ag shows a PCE of around 11%. Our best control device with PCBM layer delivered a PCE of 9.44%, with a V_{OC} of 0.81 V, a J_{SC} of 16.70 mA cm^{-2}, and an FF of 73%, which is inferior to that reported in other literatures.[29, 30] The **10a** based device showed a PCE of 6.24% with a J_{SC} of 16.30 mA cm^{-2}, a V_{OC} of 0.82 V, and an FF of 47%. **10a** showed low performance with low FF compared to the PCBM one, which could be related to several reasons, such as a higher mobility of PCBM (μ_{PCBM} = 1.22×10^{-3} cm^2 V^{-1} s^{-1}) compared to that of **10a** (μ_{10a} =1.09×10^{-4} cm^2 V^{-1} s^{-1}).

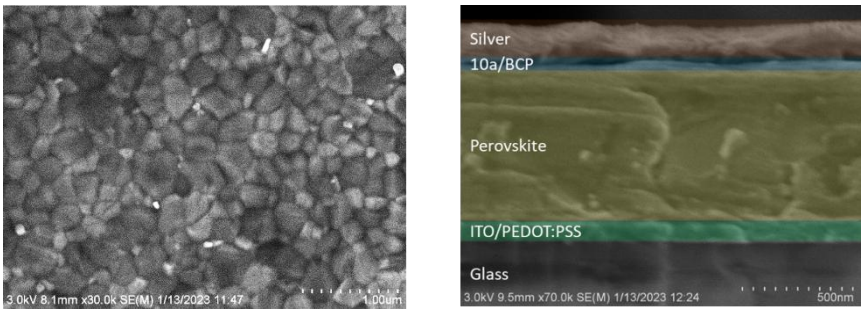

Figure 13 Top-view SEM images of the perovskite thin film deposited on the PEDOT:PSS (a); and cross sectional image of the perovskite solar cell device (b).

One of the reasons for the low value of Voc and FF for both devices could be related to the non-radiative recombination. Generally, it has been agreed that the non-radiative recombination losses arise from defects (charge-carrier traps) either in the bulk perovskite or at the interfaces.[31] Therefore, an optimization effort to passivate the defects on the perovskite surfaces and at the grain boundaries is necessary to enhance efficiency. Previous work has demonstrated that suitable small

molecules, such as D–A–D with malononitrile as acceptor moiety, can effectively passivate the perovskite via Pb–N interactions.[32, 33] To verify the passivation effect, we prepared samples: pristine perovskite film and perovskite complexed with **4** via solvent annealing process, respectively. Compared with a control cell, the devices incorporating the derivative **4** exhibited improved performance with PCE = 6.94%, Voc = 0.79 V, Jsc = 17.11 mA cm^{-2}, FF = 51%. Thus, passivation treatment improved the Jsc and FF and confirming the less nonradiative recombination in the perovskite films. The overall improvement of the PCE should be ascribed to the ability of derivative **4** to passivate various trap sites on the crystal surface and at the grain boundaries of perovskite to minimize the non-radiative charge recombination. In summary this un-optimised device was operational with a PCE around 7%. Albeit displaying lower PCE compared with a reference device using PCBM (PCE of 9%), this initial device work highlights the potential of these materials to perform as ETL in solar cells.

4 Conclusion

We provide a wide range of systematic structure-property relationships that offer new perspectives on the design of electron-acceptor materials. Appropriate chemical modifications of both π–bridge and end capped group can effectively manipulate the optical, electrochemical, and energy levels of these molecules. When the isatin ring was replaced by the isatylidene malononitrile ring, a bathochromic shift of 80-110 nm at the longest wavelength was observed, which reduced the optical band-gap. The red-shift induced by thiophene is more pronounced compared to BDT or phenyl

moiety, suggesting that thiophene has stronger intramolecular CT properties. The LUMO energy level of the malononitrile materials obtained by electrochemical measurements is around –4.00 eV, which is about 0.5 eV lower than that of bis-iastin derivatives. Changing the bridging group affects both the HOMO and LUMO energy levels of the materials, unlike the traditional view in which the donor unit mainly affects the HOMO energy level of the materials. This is also reflected in the DFT calculations where both HOMO and LUMO are fully delocalized on the two malononitrile terminal acceptor groups and the π–conjugated bridge donor segments. Meanwhile, the HOMO or LUMO energy levels of the materials obtained by DFT calculations are very close to the experimental data, with many data deviations within 0.1 eV. The material **10a** has a low LUMO energy level, near –4.0 eV, as well as a small band-gap around 1.20 eV. The introduction of nitro in dicyano bis-isatin significantly stabilizes LUMO energy level, and thus may contributes to the air stability of the material. The ability of these new A-D-A OSC to transport electrons is confirmed by the SCLC measurements. Furthermore, their utility as electron transporting materials is demonstrated in PSCs.

CRediT authorship contribution statement

Abderrahim Yassar: Supervision, Funding acquisition, Writing – original draft. **Shiwei Ren:** PhD student performed the organic synthesis of dyes. **Amirhossein Habibi:** Postdoctoral student developed the triple-cation perovskite and performed photovoltaic characterization. **Pingping Ni:** PhD student performed the organic

synthesis of dyes. **Yuexing Zhang:** carried out the theoretical calculations. **Abderrahim Yassar:** Supervised the whole project and, Funding acquisition, written the original draft. **Yuexing Zhang:** Supervised the whole project and, Funding acquisition, written the original draft. All authors have contributed in correcting, enhancing the quality of the discussion and editing the manuscript.

Declaration of competing interest

The authors declare that they have no known competing financial interests or personal relationships that could have appeared to influence the work reported in this paper.

Data availability

No data was used for the research described in the article.

Acknowledgements

This work benefited from the support of EDF in the framework of the research and teaching Chair «Sustainable energies » at Ecole polytechnique. Y. Z. gratefully thanks the financial support from the Science and Technology Research Project of Hubei Province Department of Education (D20191001), Hubei and Dezhou University. A.Y. thanks ANR-16-CE07-0024(GATE), S.R. thanks the China Scholarship Council for a PhD fellowship (No.201808070090) and the fellowship of China Postdoctoral Science Foundation No.2022TQ0399.

Appendix A. Supplementary data

Supplementary data to this article can be found online at https:

References

[1] Braga D, Horowitz G. High-Performance Organic Field-Effect Transistors. Advanced Materials. 2009;21(14-15):1473-86.
[2] Rumer JW, Schroeder BC, Nielsen CB, Ashraf RS, Beatrup D, Bronstein H, et al. Bis-lactam-based donor polymers for organic solar cells: Evolution by design. Thin Solid Films. 2014;560:82-5.
[3] Alsufyani M, Hallani RK, Wang S, Xiao M, Ji X, Paulsen BD, et al. The effect of aromatic ring size in electron deficient semiconducting polymers for n-type organic thermoelectrics. Journal of Materials Chemistry C. 2020;8(43):15150-7.
[4] Kim JH, Choi MW, Kim SY, Jung S, Choi YS, Park SY. Novel Organic Semiconductors Based on 1,5- Naphthyridine- 2,6- Dione Unit for Blue- Selective Organic Phototransistor. Advanced Optical Materials. 2020;8(20).
[5] Takagi K, Yamamoto SY, Tsukamoto K, Hirano Y, Hara M, Nagano S, et al. Synthesis and Field-Effect Transistor Application of pi-Extended Lactam-Fused Conjugated Oligomers obtained by Tandem Direct Arylation. Chemistry. 2018;24(53):14137-45.
[6] Gomaa MA, Hassan DK. Synthesis, characterization, and antimicrobial activity of some new N-aryl-N'-(2-oxoindolin-3-ylidene)-benzohydrazonamides. Arch Pharm (Weinheim). 2019;352(12):e1900209.
[7] Yousaf I, Khera RA, Iqbal J, Gul S, Jabeen S, Ihsan A, et al. Isatin-derived non-fullerene acceptors for efficient organic solar cells. Materials Science in Semiconductor Processing. 2021;121.
[8] Liu Y, Wang H, Wan J. Recent Advances in Diversity Oriented Synthesis through Isatin-based Multicomponent Reactions. Asian Journal of Organic Chemistry. 2013;2(5):374-86.
[9] Dhondge AP, Chen JY, Lin T, Yen FM, Li KW, Hsieh HC, et al. Di-2-(2-oxindolin-3-ylidene)malononitrile Derivatives for N-Type Air-Stable Organic Field-Effect Transistors. Org Lett. 2018;20(1):40-3.
[10] Dhondge AP, Tsai PC, Nien CY, Xu WY, Chen PM, Hsu YH, et al. Angular-Shaped Naphthalene Bis(1,5-diamide-2,6-diylidene)malononitrile for High-Performance, Air-Stable N-Type Organic Field-Effect Transistors. Org Lett. 2018;20(9):2538-42.
[11] Dhondge AP, Huang YX, Lin T, Hsu YH, Tseng SL, Chang YC, et al. Benzodipyrrole-2,6-dione-3,7-diylidenedimalononitrile Derivatives for Air-Stable n-Type Organic Field-Effect Transistors: Critical Role of N-Alkyl Substituent on Device Performance. J Org Chem. 2019;84(21):14061-8.
[12] Yoo D, Luo X, Hasegawa T, Ashizawa M, Kawamoto T, Masunaga H, et al.

n-Type Organic Field-Effect Transistors Based on Bisthienoisatin Derivatives. ACS Applied Electronic Materials. 2019;1(5):764-71.
[13] Zhang G, Zhao Y, Kang B, Park S, Ruan J, Lu H, et al. Fused Heptacyclic-Based Acceptor–Donor–Acceptor Small Molecules: N-Substitution toward High-Performance Solution-Processable Field-Effect Transistors. Chemistry of Materials. 2019;31(6):2027-35.
[14] Zhang G, Chen R, Sun Y, Kang B, Sun M, Lu H, et al. Improved charge transport in fused-ring bridged hemi-isoindigo-based small molecules by incorporating a thiophene unit for solution-processed organic field-effect transistors. Journal of Materials Chemistry C. 2020;8(4):1398-404.
[15] Zhao D, Hu J, Liu Z, Xiao B, Wang X, Zhou E, et al. Isatylidene malononitrile derived acceptors for fullerene free organic solar cells. Dyes and Pigments. 2018;151:102-9.
[16] Zhao D, Hu J, Cao K, Xiao B, Zhou E, Zhang Q. Isatin-derived non-fullerene acceptors towards high open circuit voltage solar cells. Dyes and Pigments. 2019;162:898-904.
[17] Shaikh DB, Ali Said A, Wang Z, Srinivasa Rao P, Bhosale RS, Mak AM, et al. Influences of Structural Modification of Naphthalenediimides with Benzothiazole on Organic Field-Effect Transistor and Non-Fullerene Perovskite Solar Cell Characteristics. ACS Appl Mater Interfaces. 2019;11(47):44487-500.
[18] Zheng S, Wang G, Liu T, Lou L, Xiao S, Yang S. Materials and structures for the electron transport layer of efficient and stable perovskite solar cells. Science China Chemistry. 2019;62(7):800-9.
[19] Zhdankin VV, Moradi R, Ziarani GM, Lashgari N. Recent applications of isatin in the synthesis of organic compounds. Arkivoc. 2017;2017(1):148-201.
[20] Becke AD. Density- functional thermochemistry. III. The role of exact exchange. The Journal of Chemical Physics. 1993;98(7):5648-52.
[21] Lee C, Yang W, Parr RG. Development of the Colle-Salvetti correlation-energy formula into a functional of the electron density. Phys Rev B Condens Matter. 1988;37(2):785-9.
[22] Miehlich B, Savin A, Stoll H, Preuss H. Results obtained with the correlation energy density functionals of becke and Lee, Yang and Parr. Chemical Physics Letters. 1989;157(3):200-6.
[23] Frisch MJ, Trucks GW, Schlegel HB, Scuseria GE, Robb MA, Cheeseman JR, et al. Gaussian 16 Rev. C.01. Wallingford, CT2016.
[24] Azeem U, Khera RA, Naveed A, Imran M, Assiri MA, Khalid M, et al. Tuning of a A-A-D-A-A-Type Small Molecule with Benzodithiophene as a Central Core with Efficient Photovoltaic Properties for Organic Solar Cells. ACS Omega. 2021;6(43):28923-35.
[25] Raynor AM, Gupta A, Plummer CM, Jackson SL, Bilic A, Patil H, et al. Significant Improvement of Optoelectronic and Photovoltaic Properties by Incorporating Thiophene in a Solution-Processable D-A-D Modular Chromophore. Molecules. 2015;20(12):21787-801.
[26] Bondi AA. van der Waals Volumes and Radii. The Journal of Physical Chemistry.

1964;68:441-51.
[27] Jean GN, Nord FF. STUDIES ON THE CHEMISTRY OF HETEROCYCLICS. XXX.1BIAROMATICS IN THE THIOPHENE SERIES. III. THE ULTRAVIOLET ABSORPTION SPECTRA OF BIPHENYL TYPE COMPOUNDS CONTAINING THE THIOPHENE RING. Journal of Organic Chemistry. 1955;20:1370-8.
[28] Zhang G, Sun M, Wang W, Qiu L. Acceptor-donor-acceptor small molecules based on fuse ring and 2-(2-oxindolin-3-ylidene)malononitrile derivatives for solution-processed n-type organic field-effect transistors. Synthetic Metals. 2019;256.
[29] Sharma S, Sakai N, Ray S, Senanayak SP, Sirringhaus H, Snaith HJ, et al. Inverted perovskite solar cells with air stable diketopyrrolopyrrole-based electron transport layer. Solar Energy. 2019;186:9-16.
[30] Mamun AA, Ava TT, Zhang K, Baumgart H, Namkoong G. New PCBM/carbon based electron transport layer for perovskite solar cells. Phys Chem Chem Phys. 2017;19(27):17960-6.
[31] Yang G, Ren Z, Liu K, Qin M, Deng W, Zhang H, et al. Stable and low-photovoltage-loss perovskite solar cells by multifunctional passivation. Nature Photonics. 2021;15(9):681-9.
[32] Daskeviciute- Geguziene S, Zhang Y, Rakstys K, Xiao C, Xia J, Qiu Z, et al. Passivating Defects of Perovskite Solar Cells with Functional Donor- Acceptor–Donor Type Hole Transporting Materials. Advanced Functional Materials. 2022;33(1).
[33] Byranvand MM, Saliba M. Defect Passivation of Perovskite Films for Highly Efficient and Stable Solar Cells. Solar RRL. 2021;5(8).